Experimental evidence of the anisotropy of tracer dispersion in rough fractures with sheared walls

A. Boschan,[1,2] H. Auradou,[1] I. Ippolito,[2] R. Chertcoff,[2] and J. P. Hulin[1]

[1] Dispersion experiments are compared for two model fractures with identical complementary rough walls but with a relative shear displacement δ parallel ($\delta \parallel \mathbf{U}$) or perpendicular ($\delta \perp \mathbf{U}$) to the flow velocity $\mathbf{U}$. The flowing fluid is a shear thinning polymer solution with a Newtonian behavior at low shear rates. For $\delta \perp \mathbf{U}$, the mixing fronts display large structures well reproduced by assuming parallel channels of conductance deduced from the aperture field. This model also explains the amplification of the structures in the shear thinning regime and the distribution of the local transit times $\bar{t}(x, y)$. For $\delta \parallel \mathbf{U}$, the front is much flatter. The local thickness of the front is characterized by a dispersivity $\alpha(x, y)$: its distribution is narrow enough to define an effective value $\alpha(Pe)$ only for $\delta \parallel \mathbf{U}$, and, in this case, $\alpha(Pe)$ has a Taylor-Aris-like variation with Pe.

[2] Channelization is a key characteristic of flow and transport in fractured rocks [*Committee on Fracture Characterization and Fluid Flow*, 1996] and results frequently from the occurence of relative shear displacements of the two fracture surfaces during fracturation [*Olsson and Brown*, 1993; *Gentier et al.*, 1997]. Such displacements (named δ thereafter) have been shown both experimentally and numerically [*Matsuki et al.*, 2006; *Auradou et al.*, 2006, 2008] to create channels and ridges perpendicular to δ. Their length depends on the multiscale geometry of the walls and, even for amplitudes δ smaller than 1‰ of the fracture length L_x, they represent a significant fraction of L_x [*Matsuki et al.*, 2006]. The permeability is then anisotropic: both its value and the correlation length of the velocity field are higher for a mean flow parallel to these channels (i.e., perpendicular to δ).

[3] The objective of the present communication is to demonstrate experimentally that this type of channelization induces a strong anisotropy of the magnitude and properties of tracer dispersion. A previous work [*Boschan et al.*, 2007] studied dispersion in a single self-affine model fracture, using several shear thinning fluids to investigate the specific influence of the rheology on the mixing front geometry and local/global dispersion properties. In this work, we use always the same fluid but we compare dispersion measurements in two different fracture models: both are made of the same pair of complementary surfaces but with a relative shear displacement respectively perpendicular and parallel to the mean flow velocity leading to different orientations of

the channels. Our work is then focused on the dependence of dispersion on the relative orientation of the channels and the mean fluid velocity $\mathbf{U}$. The flowing fluid is a polymer solution with a high constant viscosity at low shear rates (Newtonian plateau) which stabilizes the flow with respect to buoyancy driven instabilities at low velocities [*Tenchine and Gouze*, 2005]. At high shear rates the fluid has shear thinning rheological characteristics: this will be shown to enhance the velocity contrasts in the flow field and make the observation of the anisotropy easier. Moreover, dispersion in shear thinning fluids is relevant to water management processes using concentrated colloidal suspensions, emulsions and liquid foams.

[4] Many experiments on solute spreading in fractures have been reported: *Keller et al.* [1999] and *Lee et al.* [2003] observed dispersion coefficients D increasing linearly with the velocity $\mathbf{U}$ (i.e., the dispersivity $\alpha = D/U$ is constant). *Neretnieks et al.* [1982] have also demonstrated that the variation of the breakthrough curve is not continuous but displays steps indicating that preferential channels were present in the fracture: information on the development of the mixing zone with the distance will help identify such flow channelization effects and their influence on tracer dispersion. Measurements by *Park et al.* [1997] used radioactive tracers, still with a resolution too low to investigate local spreading. In all these papers, the anisotropy of dispersion is not investigated and (except for work by *Lee et al.* [2003]), little information is available on the relative position of the fracture walls.

[5] We use transparent model fractures allowing for optical concentration measurements [*Boschan et al.*, 2007]. Fluid flow takes place between two self-affine rectangular rough walls mounted vertically and of same characteristic exponent $H = 0.8$ as in many fractured rocks [*Poon et al.*, 1992]. The mean flow velocity $\mathbf{U}$ is parallel to the length $L_x = 350$ mm of the walls (their width is $L_y = 90$ mm).

---

[1]Laboratoire Fluide, Automatique et Systèmes Thermiques, UMR7608, Université Paris 6 and 11, Université Paris Sud, CNRS, Orsay, France.
[2]Grupo de Medios Porosos, Departamento de Física, Facultad de Ingeniería, Universidad de Buenos Aires, Buenos Aires, Argentina.
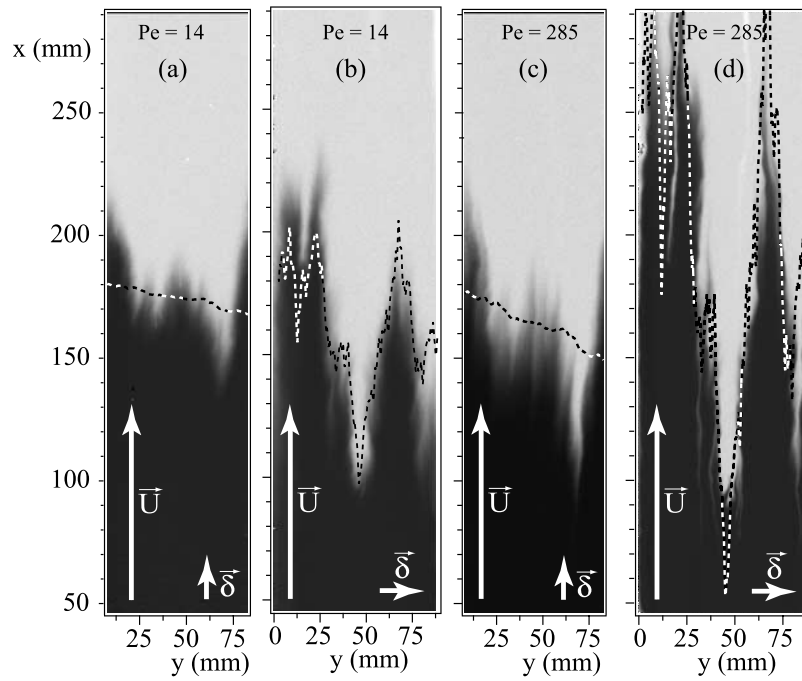
Figure 1. Gray level maps of the relative concentration c of the displaced fluid in the two transparent models (white, $c = 1$; black, $c = 0$; dashed lines, theoretical front profiles calculated from equation (1); δ is the relative shear displacement between the walls): (a and c) $\delta \parallel \mathbf{U}$ and (b and d) $\delta \perp \mathbf{U}$. Mean velocities are $U = 0.0125$ mm s^{-1} ($Pe = 14$) in Figures 1a and 1b and $U = 0.25$ mm s^{-1} ($Pe = 285$) in Figures 1c and 1d. The maps correspond to the time when the injected volume of displacing fluid is half the void space. The vertical and horizontal axes show the distance from the left and inlet sides of the model, respectively.

[6] The surfaces bounding the fracture gap are exactly complementary. The aperture field used in the experiments is obtained by first introducing a normal displacement between them (the mean aperture is equal to its magnitude) and, then, a lateral shear displacement δ parallel or perpendicular to $\mathbf{U}$ (i.e., to x). Because of this shear, the local aperture $a(x, y)$ varies spatially since matching features of the two walls do not correspond to same (x, y) values any more. As mentioned above, this leads to the appearance of channels respectively perpendicular and parallel to $\mathbf{U}$. Both δ and the mean aperture a are equal to 0.75 mm and the standard deviation of the aperture is $\sigma_a = 0.144$ mm. The flow field is therefore more channelized than in the model of *Boschan et al.* [2007] in which $\sigma_a = 0.11$ mm (for $\delta = 0.33$ mm). The statistical properties of the aperture fields of similar fractures are discussed in detail by *Auradou et al.* [2006, 2008].

[7] The fluid is a shear thinning 1000 ppm solution of scleroglucan in water and its rheological properties are discussed by *Boschan et al.* [2007]. At low shear rates ($\dot\gamma \leq \dot\gamma_0 = 0.026$ s^{-1}), the viscosity is constant with a high value ($\mu = \mu_0 \approx 4500$ mPa s). For a viscous Newtonian flow between parallel plates at a distance a, the mean velocity for which the shear rate at the walls is equal to $\dot\gamma_0$ is $U_0 = a\dot\gamma_0/6 = 3 \times 10^{-3}$ mm s^{-1}. For $\dot\gamma \geq \dot\gamma_0$, the viscosity decreases as $\mu \propto \dot\gamma^{n-1}$ with $n = 0.26$. The displacement process is visualized by adding 0.2 g L^{-1} of blue dye to the displacing solution. The densities are matched by adding NaCl to the displaced solution saturating initially the model; measurements in the reverse configuration were also performed to check that no buoyancy effects are present.

[8] The flow velocity U is kept constant during each experiment with: $0.0024 \leq U \leq 0.24$ mm s^{-1} and the transport of dye is characterized by the dimensionless Péclet number $Pe = Ua/D_m$, where $D_m = 6.5 \ 10^{-10}$ mm s^{-1} is the molecular diffusion coefficient of the tracer. Dye concentration maps are obtained from light absorption measurements [see *Boschan et al.*, 2007]: the high resolution of these maps (typically 0.2 mm per pixel) allows one to analyze simultaneously the dispersion process at the local and global scales.

[9] Figure 1 shows maps obtained in the two model fractures at two different velocities U. If $\delta \perp \mathbf{U}$, two fingers soar upward with a large trough in between (Figures 1b and 1d): they correspond to faster paths parallel to $\mathbf{U}$ (Figure 1b) and their amplitude increases with U. For $\delta \parallel \mathbf{U}$, the front is smoother (Figures 1a and 1c) while its mean slope and the size of the indentations still increase with the velocity.

[10] The large structures in Figures 1b and 1d reflect velocity contrasts between channels created by the shear. They are well reproduced by modeling the fracture aperture field as a set of independent parallel channels of aperture $a(y) = \langle a(x, y)\rangle_x$. A particle starting at a transverse distance y at the inlet should move at a velocity proportional to $a(y)^{(n+1)/n}$ where $n = 0.26$ for $U > U_0$ and $n = 1$ for $U < U_0$. The profile $x_f(y, t)$ of the front at a time t is then

$$x_f(y,t) = \frac{\overline{x}(t) \ a(y)^{(n+1)/n}}{\langle a(y)^{(n+1)/n}\rangle_y},$$ (1)

where $\overline{x}(t) = \langle x_f(y, t)\rangle_y$ and $\langle a(y)^{(n+1)/n}\rangle_y$ are averages calculated over y [see *Auradou et al.*, 2006, equation (7);
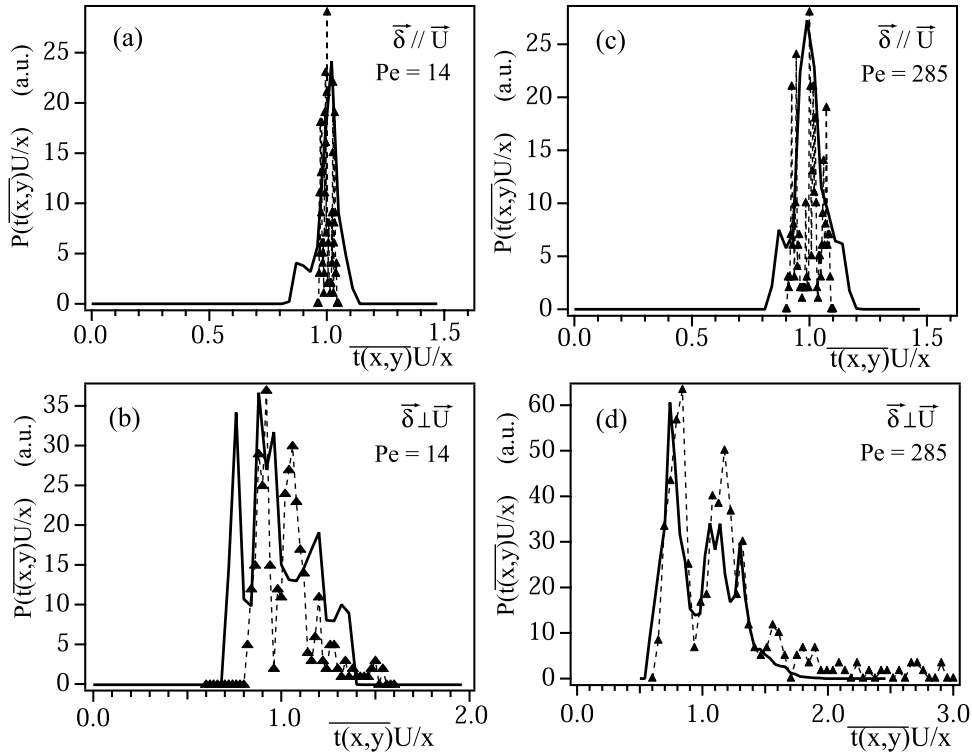
Figure 2. Histograms of the experimental normalized local transit time $\bar{t}(x, y)U/x$ (solid lines) for the same models and *Pe* values as in Figure 1. The distribution of $\bar{t}(x, y)U/x$ has been computed in the upper fifth of the length of the model to make meaningful comparisons with the distribution of the theoretical transit times (solid triangles and dashed lines) determined from equation (1).

Auradou et al., 2008, equations (5)−(8)]. The profiles computed using equation (1) and the actual aperture fields appear in Figures 1a−1d as dashed lines; from the above discussion, one assumed that $n = 1$ at the lowest velocity (Figures 1a and 1b) and $n = 0.26$ at the highest one (Figures 1c and 1d). Equation (1) predicts well the location and shape of the "fingers" and "troughs" at both velocities for $\boldsymbol{\delta} \perp \mathbf{U}$ although their amplitude is slightly underestimated in Figure 1b. In this latter case, one has $U \sim U_0$, corresponding to a transition regime between the power law and Newtonian rheologies.

[11] For $\boldsymbol{\delta} \parallel \mathbf{U}$, the features of the front are also visible at the same transverse distances y in Figures 1a and 1c: they reflect again a convective spreading of the front due to velocity contrasts between the flow paths. However, in contrast with the previous case $\boldsymbol{\delta} \perp \mathbf{U}$, these features (except for the small global slope of the front) are not reproduced by the theoretical model (dashed line): this was to be expected since its underlying hypothesis are not satisfied for $\boldsymbol{\delta} \parallel \mathbf{U}$.

[12] The time variations of the local concentration $c(x, y, t)$ on individual pixels provide additional, more quantitative, information on the convective and diffusive processes involved. Practically, the variation of the normalized concentration $c(x, y, t)$ with time is well fitted by the function

$$c(t) = \frac{1}{2}\left(1 + erf\frac{t - \bar{t}}{\sqrt{4Dt/U^2}}\right). \tag{2}$$

Mathematically this function is the classical solution of the convection-diffusion equation in an homogeneous medium following a step-like initial variation of the concentration, uniform in the direction transverse to the flow. In the present medium which is heterogeneous, $\bar{t}$ and D are only used to characterize the transit time of the front from the inlet to an individual pixel (x,y) and its local width as it reaches this pixel. For each experiment the coefficients $\bar{t}(x, y)$ and $D(x, y)$ are determined for all points (x, y) inside the field of view. The displacement front includes at a time t the set of points for which $\bar{t}(x, y) = t$ [*Boschan et al.*, 2007]. The coefficient $D(x, y)$ is determined from the centered second moment $\overline{\delta t^2}(x, y)$ of the transit times at the point (x, y) and provides information on the local thickness of the front as it reaches this point. In the following, $\alpha(x, y) = D(x, y)/U$ will be called: "local dispersivity."

[13] Figure 2 compares the experimental and theoretical probability distributions of the normalized times $\bar{t}(x, y) \, U/x$ for the same experiments as Figure 1. The above model predicts that the normalized time is related to the aperture of the channels by: $\bar{t}(x, y) \, U/x = x_f (y, t)/\bar{x}(t)$, in which the ratio $x_f (y, t)/\bar{x}(t)$ is given by equation (1). The distribution is then obtained from the histogram of the results for all y values.

[14] As expected, these distributions are much broader for $\boldsymbol{\delta} \perp \mathbf{U}$ (Figures 2b−2d) than for $\boldsymbol{\delta} \parallel \mathbf{U}$ (Figures 2a−2c). For $Pe = 285$, the experimental distribution for flow parallel to the channels coincides very well with the theoretical one and displays two peaks reflecting the structuration of the flow. At $Pe = 14$, the width and global shape of the experimental and theoretical distributions are overall similar
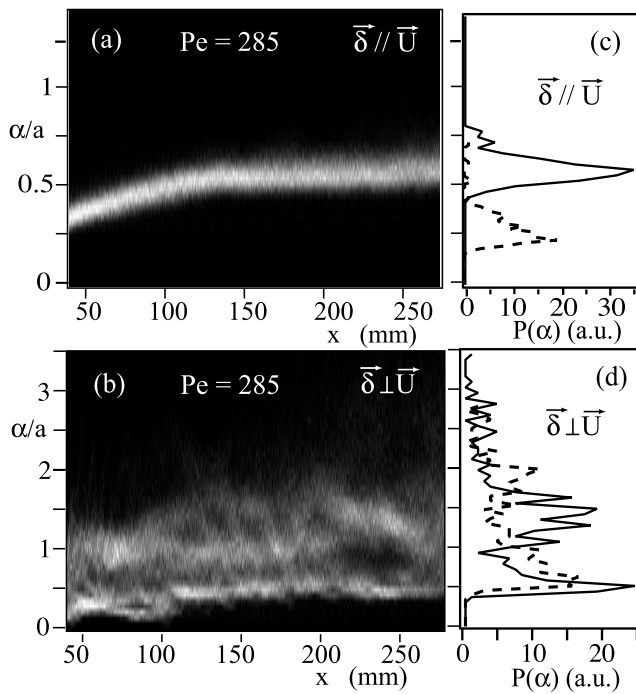
Figure 3. (a and b) Histograms (gray levels) of the values of the normalized local dispersivity $\alpha(x, y)/a$ (vertical scale) as a function of the distance x (horizontal scale). White, maximum probability; black, zero probability. (c and d) Histograms obtained at $x = 240$ mm for $Pe = 285$ (solid line) and $Pe = 14$ (dashed line).

and narrower than for $Pe = 285$ because of the lower-velocity contrast in the Newtonian limit. For $\delta \parallel U$ (Figures 2a–2c), the distribution at both Péclet numbers is much narrower than for $\delta \perp U$. The mean peak corresponds to $\bar{t}(x, y)U/x \simeq 1$; its width increases with Pe (again likely due to an increase of the velocity contrasts) and is similar to that of the theoretical distributions. Still for $\delta \parallel U$, the experimental distribution displays additional "aisles": these reflect likely complex paths deviating from straight trajectories parallel to U.

[15] From the above results, the overall geometry of the mixing front seems to be determined mainly by convective effects; we examine now the relative influence of convection and diffusion on the local width of the front through the variation of $\alpha(x, y)$ with Pe. Figures 3a and 3b display, for each value of x (horizontal scale), the histogram (coded in grey levels) of the corresponding values of $\alpha(x, y)/a$ (vertical scale).

[16] For $\delta \parallel U$, the probability distribution of $\alpha(x, y)/a$ is narrow, particularly at high flow velocities (Figures 3a and 3c). Moreover, its mean value $\alpha(Pe)/a$ varies little with the distance x and becomes constant for $x \geq 100$ mm (see inset of Figure 4). The increase with time of the local front thickness is therefore diffusive and the corresponding normalized dispersivity will be taken equal to $\alpha(Pe)/a$.

[17] The variation of $\alpha(Pe)$ with Pe for $\delta \parallel U$ displayed in Figure 4 provides quantitative information on the mechanisms governing the increase of the local front thickness with distance: the values are compared to theoretical predictions (dashed and solid lines) including both the effects of Taylor dispersion [*Taylor*, 1953] and molecular diffusion and assuming respectively $n = 1$ [*Aris*, 1956] and $n = 0.26$.

Overall the experimental values are similar (although slightly higher) to the predictions for $n = 0.26$ with a dominant Taylor dispersion component at high Pe values ($\alpha(Pe)/a \propto Pe$). At low Pe values, the values obtained for $n = 1$ (dashed line) and for $n = 0.26$ are similar and the dispersivity is increasingly influenced by a molecular diffusion component ($\alpha(Pe)/a \simeq 1/Pe$). A similar contribution of Taylor dispersion at high Pe values has already been demonstrated in models with a randomly distributed aperture of short correlation length [*Detwiler et al.*, 2000]; however, at low Pe values, these authors did not observe a transition toward molecular diffusion ($\alpha \propto (1/Pe)$) but a geometrical dispersion regime characterized by $\alpha = cst(Pe)$) and reflecting spatial fluctuations of the velocity due to those of the aperture.

[18] For $\delta \perp U$ (Figures 3b and 3d), the distribution of the values of α/a is much broader with a "tail" at large values of α/a and two peaks at high velocities (solid curve in Figure 3): in contrast to the case $\delta \parallel U$, no single value of α/a characterizes well the whole distribution. The value corresponding to the first peak seems to reach a limit at long distances x: it corresponds likely to fluid paths for which Taylor-Aris dispersion is dominant compared to the influence of transverse velocity gradients, at least at high Pe values. The corresponding values of α/a are plotted in Figure 4 (solid squares): they are close to those corresponding to Taylor dispersion (and to the other model) at high Pe values but higher at low Pe values.

[19] Comparing the dispersion characteristics discussed above demonstrates their very strong dependence at both the global and local scales on the orientation of the mean flow with respect to the channels created by the shear. At the global scale, the front displays large-scale fingers and troughs for $\delta \perp U$ (i.e., U parallel to the channelization);
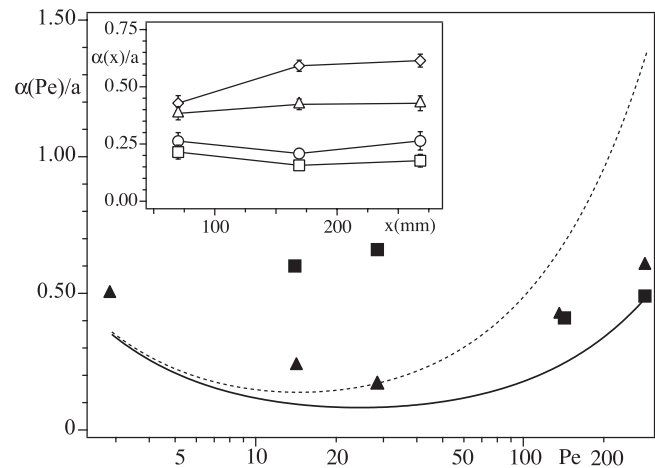
Figure 4. Variation of the normalized local dispersivity α/a as a function of Pe (solid triangles, mean value of α/a for $\delta \parallel U$; solid squares, value corresponding to the first peak in the distribution of α/a for $\delta \perp U$; solid and dashed lines, Taylor-Aris dispersivity between parallel plates for a power law fluid of exponent $n = 0.26$ and for a Newtonian fluid with $n = 1$, respectively). Inset shows the variation of the mean value $\langle \alpha(x, y) \rangle_y$ as a function of the distance x for $\delta \parallel U$: $Pe = 285$ (open diamonds), $Pe = 142$ (open triangles), $Pe = 28.5$ (open squares), and $Pe = 14$ (open circles).

these features are well reproduced by a channel model using a transverse effective permeability profile derived from the aperture field. Moreover, the increase of the size of the fingers between low and high Pe values is well predicted from the variations of the fluid rheology with Pe (shear thinning at high Pe values and Newtonian at low ones). For $\delta \parallel \mathbf{U}$ (i.e., $\mathbf{U}$ perpendicular to the channelization), the front is much flatter, suggesting a more effective sampling of the velocity heterogeneities by solute particles. The remaining distortions of the front cannot be predicted by the channel model: however, they are observed at the same transverse locations at all velocities and remain of similar amplitudes (taking into account the variations of the rheology). This suggests that these features are of convective origin in all cases.

[20] While these data agree with the numerical study of *Auradou et al.* [2006] and, for $\delta \perp \mathbf{U}$, with the experiments of *Auradou et al.* [2008], the present work expands the range of validity of these previous results to more heterogeneous media and large-scale distortions of the front. Further information related to the front propagation has also been obtained from the distribution of the local normalized transit times $\bar{t}(x, y)U/x$. These distributions are much broader for $\delta \perp \mathbf{U}$ than for $\delta \parallel \mathbf{U}$ and their width is larger in the shear thinning regime: like the front geometry, they are well predicted from the channel model but only if $\delta \perp \mathbf{U}$.

[21] From the practical point of view, these results demonstrate the interest of analyzing the transit time distributions at different distances x along the flow instead of performing only a measurement at the outlet. In the case $\delta \perp \mathbf{U}$, for instance, the mean square width $\overline{\delta t^2}$ of the transit time distribution scales as $1/U^2$ (see Figures 2b–2d); the same velocity scaling would be found for pure geometrical dispersion. In contrast, the dependence of $\overline{\delta t^2}$ on the distance x from the inlet is different: $\propto x^2$ in the first case and $\propto x$ in the second. Measurements at different x values allow one therefore to identify unambiguously the spreading process (although channeling effects may already be suggested by steps in the concentration variation curves [*Neretnieks et al.*, 1982]).

[22] Analyzing now the increase of the local front thickness with distance, a strong dependence of the distribution of the values of $\alpha(x, y)$ on the orientation of δ is also observed. For $\delta \perp \mathbf{U}$ the distribution is much broader than for $\delta \parallel \mathbf{U}$ (and also than for the model of *Boschan et al.* [2007] with $\delta \perp \mathbf{U}$ and a smaller relative shear displacement δ): no single dispersivity can be defined and even the lowest local values of $\alpha(x, y)$ (corresponding to simple flow paths) are larger, except at high Pe values, than those of *Boschan et al.* [2007] which reflected Taylor-Aris dispersion. This is likely due to the enhancement of dispersion by the exchange of tracer (due to transverse molecular diffusion) between adjacent flow paths of different velocities. For $\delta \parallel \mathbf{U}$, the variation of the local front thickness is diffusive and may be characterized by the mean value $\alpha(Pe)$ of the distribution: the variation of $\alpha(Pe)$ with Pe is mostly due to Taylor-Aris dispersion as in the work by *Boschan et al.* [2007]. Finally, like in this latter work, and unlike for rough fractures with a small correlation length of the aperture [*Detwiler et al.*, 2000], no geometrical regime characterized by a diffusive local front spreading and a dispersivity $\alpha = cst(Pe)$ is observed in either model.

[23] This set of results may be transposed to the interpretation of field observations [see, e.g., *Becker and Shapiro*, 2000] within the limitations associated to the restricted length of the samples used and the fact that the relatively small standard deviations considered in this study may not allow to reproduce fully the effects of mass transfer between rapid and slow channels in a broader distribution of conductivities. For much longer fractures, transverse diffusion might be large enough for solute particles to sample the whole distribution of local velocities and reach such a global diffusive spreading regime. Also, for higher standard deviations of the aperture, more complex models of dispersion should be considered [*Bouchaud et al.*, 1987; *Dentz et al.*, 2008]. Because of the specific correlations of the flow velocity field for self-affine wall geometries [*Auradou et al.*, 2006], the corresponding exponent would then likely depend on the characteristic roughness exponent of the fracture walls.

References

Aris, R. (1956), On the dispersion of a solute particle in a fluid moving through a tube, *Proc. R. Soc. London, Ser. A*, *235*, 67–77.

Auradou, H., G. Drazer, A. Boschan, J. P. Hulin, and J. Koplik (2006), Shear displacement induced channelization in a single fracture, *Geothermics*, *35*, 576–588.

Auradou, H., A. Boschan, R. Chertcoff, S. Gabbanelli, J. P. Hulin, and I. Ippolito (2008), Enhancement of velocity contrasts by shear thinning solutions flowing in a rough fracture, *J. Non Newtonian Fluid Mech.*, *153*, 53–61.

Becker, M., and A. Shapiro (2000), Tracer transport in fractured crystalline rock: Evidence of nondiffusive breakthrough tailing, *Water Resour. Res.*, *36*, 1677–1686.

Boschan, A., H. Auradou, I. Ippolito, R. Chertcoff, and J. P. Hulin (2007), Miscible displacement fronts of shear thinning fluids inside rough fractures, *Water Resour. Res.*, *43*, W03438, doi:10.1029/2006WR005324.

Bouchaud, J. P., A. Georges, and P. Le Doussal (1987), Diffusion anormale dans les milieux désordonnés: Piégeage, corrélations et théorèmes de la limite centrale, *J. Phys. France*, *48*, 1855–1860.

Committee on Fracture Characterization and Fluid Flow (1996), *Rock Fractures and Fluid Flow: Contemporary Understanding and Applications*, Natl. Acad., Washington, D. C.

Dentz, M., T. Le Borgne, and J. Carrera (2008), Effective transport in random shear flows, *Phys. Rev. E*, *77*, 020101.

Detwiler, R., H. Rajaram, and R. J. Glass (2000), Solute transport in variable aperture fractures: An investigation of the relative importance of Taylor dispersion and macrodispersion, *Water Resour. Res.*, *36*, 1611–1625.

Gentier, S., E. Lamontagne, G. Archambault, and J. Riss (1997), Anisotropy of flow in a fracture undergoing shear and its relationship to the direction of shearing and injection pressure, *Int. J. Rock Mech. Min. Sci.*, *34*, 412.

Keller, A. A., P. V. Roberts, and M. J. Blunt (1999), Effect of fracture aperture variations on the dispersion of contaminants, *Water Resour. Res.*, *35*, 55–63.

Lee, J., J. M. Kang, and J. Choe (2003), Experimental analysis on the effects of variable apertures on tracer transport, *Water Resour. Res.*, *39*(1), 1015, doi:10.1029/2001WR001246.

Matsuki, K., Y. Chida, K. Sakaguchi, and P. W. J. Glover (2006), Size effect on aperture and permeability of a fracture as estimated in large synthetic fractures, *Int. J. Rock Mech. Min. Sci.*, *43*, 726–755.

Neretnieks, I., T. Eriksen, and P. Tahtinen (1982), Tracer movement in a single fissure in granite rock: Some experimental results and their interpretation, *Water Resour. Res.*, *18*, 849–858.

Olsson, W. A., and S. R. Brown (1993), Hydromechanical response of a fracture undergoing compression and shear, *Int. J. Rock Mech. Min. Sci. Geomech. Abstr.*, *30*(7), 845–851.

Park, C. K., T. T. Vandergraaf, D. J. Drew, and P. S. Hahn (1997), Analysis of the migration of nonsorbing tracers in a natural fracture in granite using a variable aperture fracture model, *J. Contam. Hydrol.*, 26, 97–108.

Poon, C., R. Sayles, and T. Jones (1992), Surface measurement and fractal characterization of naturally fractured rocks, *J. Phys. D Appl. Phys.*, 25, 1269–1275.

Taylor, G. I. (1953), Dispersion of soluble matter in solvent flowing slowly through a tube, *J. Fluid Mech.*, 219, 186–203.

Tenchine, S., and P. Gouze (2005), Density contrast effects on tracer dispersion in variable aperture fractures, *Adv. Water Resour.*, 28, 273–289.

————————————

H. Auradou, A. Boschan, and J. P. Hulin, Laboratoire Fluide, Automatique et Systèmes Thermiques, UMR7608, Université Paris 6 and 11, Université Paris Sud, CNRS, Bâtiment 502, F-91405 Orsay CEDEX, France. (hulin@fast.u-psud.fr)

R. Chertcoff and I. Ippolito, Grupo de Medios Porosos, Departemento de Física, Facultad de Ingeniería, Universitad de Buenos Aires, Paseo Colón 850, 1063 Buenos Aires, Argentina.